

Article

# Microstructure of Semi-Solid Billets Produced by Electromagnetic Stirring and Behavior of Primary Particles during the Indirect Forming Process

Chul Kyu Jin 

School of mechanical engineering, Kyungnam University, 7 Kyungnamdaehak-ro, Masanhappo-gu, Gyeongsangnam-do, Changwon-si 51767, Korea; cool3243@kyungnam.ac.kr; Tel.: +82-55-249-2346; Fax: +82-505-999-2160

Received: 18 February 2018; Accepted: 12 April 2018; Published: 15 April 2018



**Abstract:** An A356 alloy semi-solid billet was fabricated using electromagnetic stirring. After inserting the semi-solid billet into an indirect die, a thin plate of 1.2 mm thickness was fabricated by applying compression. The microstructure of the semi-solid billets fabricated in various stirring conditions (solid fraction and stirring force) were analyzed. The deformation and behavior of the primary  $\alpha$ -Al particles were analyzed for various parameters (solid fraction, die friction, compression rate, and compression pressure). In the stirred billets, a globular structure was dominant, while a dendrite structure was dominant in the unstirred billets. As the solid fraction decreased and the stirring current increased, the equivalent diameter and roundness of the primary  $\alpha$ -Al particles decreased. The primary  $\alpha$ -Al particle sizes were reduced as the compressing velocity increased, while a greater number of particles could move as the compressing pressure increased. As the path over which the motion occurred became smoother, the fluidity of the particles improved. Under compression, bonded primary  $\alpha$ -Al particles became separated into individual particles again, as the bonds were broken. As wearing caused by friction and collisions between the particles during this motion occurred, the particle sizes were reduced, and the particle shapes become increasingly spheroid.

**Keywords:** semi-solid material; A356 alloy; electromagnetic stirring; compression; primary  $\alpha$ -Al particle

## 1. Introduction

The semi-solid forming process, which incorporates the advantages of the casting and forging processes, uses semi-solid billet, in which both solid and liquid states coexist. Flemings and Metz (1970) described the rheological behavior by a series of experiments [1]. When a material is being fabricated into a semi-solid state, the primary  $\alpha$  particle sizes can be reduced, and their shapes can be rendered almost spherical through the application of external factors such as stirring and vibration.

A number of methods have been introduced to control the crystal grain and particle growth processes when the liquid is solidified into a semi-solid state. The most common and effective techniques are material rotation methods, such as the mechanical stirring method, which uses an impeller and a screw. Spencer et al. (1972) investigated the rheological behavior of Sn-15 pct Pb alloy by using mechanical stirring. They announced that the rheological behavior of partially solidified sheared alloy has many characteristics of thixotropic slurries [2]. Fan et al. (2005) adopted the rheo-diecasting process with twin screw for manufacturing near-net shape components. They investigated the microstructure and mechanical properties of rheo-diecasting aluminum alloys under as-cast, and various heat treatment conditions [3]. Biswas et al. (2006) used an external magnetic field to achieve a strong stirring effect on the melt motion. They investigated the effect of melt convection during the solidification of Ti<sub>45</sub>Al<sub>55</sub> alloys [4]. Nafisi et al. (2006) and Bae et al. (2007) fabricated a semi-solid metal

slurry of Al–Si alloy by using electromagnetic stirring (EMS), which uses an electromagnetic field. Nafisi et al. investigated the effects of process parameters such as cooling rate and superheat on the morphology and distribution of eutectic silicon- and iron-based intermetallics during EMS. Bae et al. fabricated knuckles using semi-solid slurry by EMS [5,6]. Tzimas and Zavaliangos (2000) used a stress-induced and melt-activated (SIMA) object, which reheated and recrystallized a cold-worked billet [7]. Haga and Suzuke (2001) used a cooling slope method, which generates nuclei by allowing a material to flow on a sloped plane plate [8]. Zhang et al. (2009) developed an ultrasonic treatment method which uses powerful ultrasonic waves to create intense convection through gas bubbles [9]. Canyook et al. (2012) developed a gas-induced semi-solid (GISS) method, which uses gas bubbles [10]. As regards chemical methods, Nafisi et al. (2006) proposed a chemical grain refining method which requires a grain refiner to be added to the material [11].

Of the approaches listed above, the electromagnetic stirring method can be the most effective technique, having more advantages than disadvantages. The stirring force is weak compared to that of the mechanical stirring method, and the problems that affect the mechanical stirring method do not occur in this technique. The other advantages of this method are that fabrication is relatively simple, and it can be used as an integrated technique by easily combining it with a forming device such as a press and a casting machine. To date, a number of studies have been conducted on stirring variables that can control the crystal grains of an aluminium semi-solid slurry using the electromagnetic stirring method. In the physical experiments of Bae et al. (2007) and Oh et al. (2008), the solid particle sizes and roundness were found to change in response to the stirring conditions [6,12]. The effect of the electromagnetic stirring was confirmed, since the results showed that smaller size and higher roundness of the solid particles in semi-solid slurry were obtained when electromagnetic stirring was applied, compared with the characteristics of unstirred semi-solid slurry. The majority of studies about semi-solid materials reported that the physical mechanism behind crystal grain control is the separation and remelting of the dendrite arms, which is caused by the destruction of the initial dendrite structure due to vigorous stirring. This fragmentation or remelting mechanism theory is based on a result obtained following the application of mechanical stirring, in which the shear deformation and shearing strain rate are quite large, and the solid and liquid phases coexist in the same state. In the electromagnetic stirring method, which has a relatively weak stirring force, it is almost impossible to operate stirring in a semi-solid state with coexisting solid and liquid phases. The electromagnetic stirring must be performed in a liquid state. No study has yet produced results that can explain the mechanism through which the crystal grains are controlled by the electromagnetic stirring from the initial solidification stage.

The microstructure of A356 alloy semi-solid billet was analyzed through the application of various stirring conditions (solid fraction of billet and stirring force) of the electromagnetic stirrer. After inserting the fabricated semi-solid billet into a compression forming die, a thin plate of 1.2 mm thickness was fabricated. The deformation and behavior of the primary  $\alpha$ -Al particles were analyzed for various compression conditions (solid fraction of billet inserted into the die, die lubrication, velocity and pressure of the punch-compressing billet). The formability and mechanical properties of the thin plate according to the process conditions were analyzed.

## 2. Experimental Procedure

### 2.1. Fabrication of the Semi-Solid Billet

Semi-solid billets were fabricated through the application of electromagnetic field stirring, as aluminum in a liquid state was in the process of solidifying into a semi-solid state. Billets of 35, 45, and 55% solid fraction were fabricated under currents of 60 A. The billets with 45% solid fraction were fabricated under applied currents of 30, 60, and 90 A, respectively, so that the effects of stirring forces with varied magnitude could be examined.

### 2.1.1. Electromagnetic Stirrer

The electromagnetic stirrer was a horizontal electromagnetic stirrer fabricated with three-phase (T, S, R) three poles. The schematic diagram showing the electromagnetic stirrer setup is shown in Figure 1. A molten metal container is required for the semi-solid billet fabrication process using the electromagnetic stirrer. The container must not melt or become deformed at temperatures above 700 °C and must not be affected by the electromagnetic force. Stainless steel 304 with austenite structure, which is a nonmagnetic material, was used. A container of 100 mm height,  $\Phi 56$  mm external diameter, and 2 mm thickness was fabricated.

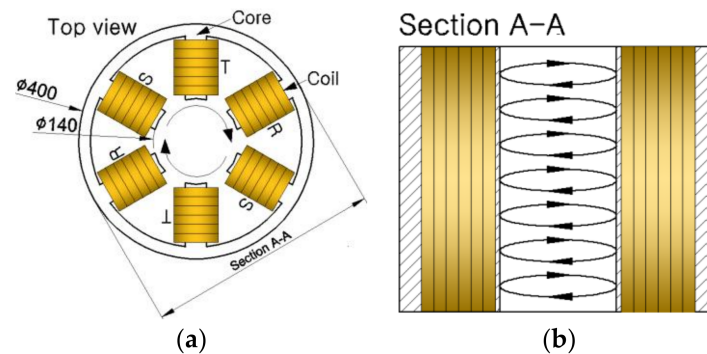


**Figure 1.** Schematic diagram of the electromagnetic stirring (EMS) device: (a) Top view; (b) Section A-A review.

### 2.1.2. Parameters of Electromagnetic Stirring

The material used in the semi-solid billet fabrication experiment was A356 alloy. The chemical composition of the A356 alloy is shown in Table 1. The solid fractions of the A356 material at different temperatures were obtained through differential scanning calorimetry (DSC). The liquidus and solidus temperatures were 617 and 547 °C, respectively, and the solidification range was 70 °C. The temperature at which a 35% solid fraction was obtained was 600 °C, while the temperatures for 45% and 55% solid fractions were 590 and 578 °C, respectively. An A356 alloy ingot was transformed into the molten state by being placed in a furnace and heated to 730 °C.

**Table 1.** Chemical composition of A356 alloy (wt %).

Si	Mg	Ti	Fe	Ni	Mn	Zn	Pb	Al
7.08	0.35	0.17	0.08	0.07	0.01	0.01	0.01	Bal.

With respect to the semi-solid billet fabrication sequence, first, the container was inserted into the electromagnetic stirrer. The container was then positioned at the center of the electromagnetic stirrer by placing a 100-mm-thick thermal insulator pad inside the stirrer and then placing the container on the pad. Next, using a ladle, the molten metal contained in the furnace was added to the container (filled to a height of 90 mm) and, immediately, stirring was initiated. Simultaneously, a thermocouple was inserted at the center of the molten metal in the container, and the temperature was measured. When the material was solidified (air cooling) at the necessary temperature for the required solid fraction, the fabricated semi-solid billet was removed from the stirrer and, as immediately as possible, cooled in water. After cooling, the primary  $\alpha$ -Al particles and liquid inside the semi-solid billet formed primary  $\alpha$ -Al particles and eutectic structures, respectively, at room temperature. The stirring conditions for the semi-solid billet fabrication process are shown in Table 2. The temperature at which the stirring was initiated was set to 620 °C, which is 3 °C higher than the liquidus temperature of the A356 alloy. Conditions 1–6 in Table 2 are different solid fractions. For conditions 1–3, billets of 35 ( $T = 600$  °C), 45 ( $T = 590$  °C), and 55% solid fraction ( $T = 578$  °C) were fabricated by stirring under

60 A. Under conditions 4–6, billets with 35%, 45%, and 55% solid fraction, respectively, were fabricated without stirring. Conditions 7 and 8 are the different stirring currents. To that end, billets with 45% solid fraction were fabricated by applying 30 A (condition 7) and 90 A (condition 8).

**Table 2.** Fabrication conditions of semi-solid billets.

No.	Temperature (°C)/Solid Fraction (%)	Stirring	Stirring Current (A)
1	600/35	Yes	60
2 (standard)	590/45	Yes	60
3	578/55	Yes	60
4	600/35	No	-
5	590/45	No	-
6	578/55	No	-
7	590/45	Yes	30
8	590/45	Yes	90

## 2.2. Thin-Plate Forming Process

After putting a semi-solid billet into the die for thin plate, the compression was conducted using a punch. A thin plate of 1.2 mm thickness was fabricated by varying the solid fraction of the billet, die lubrication, and velocity and pressure of the punch for compressing the billet.

### 2.2.1. Die and Punch

To analyze the deformation and behavior of the primary  $\alpha$ -Al particles when the semi-solid billet was compressed by the punch, an indirect closed die for thin plate was fabricated. A schematic diagram of the indirect die and punch used for the fabrication of the thin plate is shown in Figure 2. The left-hand side shows the structures of the die and punch, while the right-hand side shows the die cavity shape. The structure of the indirect die allows the semi-solid billet to be compressed by the punch when the top and bottom die are closed. A thin plate can be formed by filling the die cavity with the compressed billet. The punch compressing the semi-solid billet was 60 mm in diameter, while the die cavity size was 265 and 185 mm. A concavo-convex space 0.3 mm in depth was present at the center of the cavity. The die was installed on a 200 ton oil hydraulic press, and the punch was connected to the oil hydraulic cylinder. The load was controlled by the rate of oil discharge. Cartridge heaters were inserted in the die heating hole and preheated to approximately 270 °C. During the experiment, the die temperature was maintained at 250 °C.

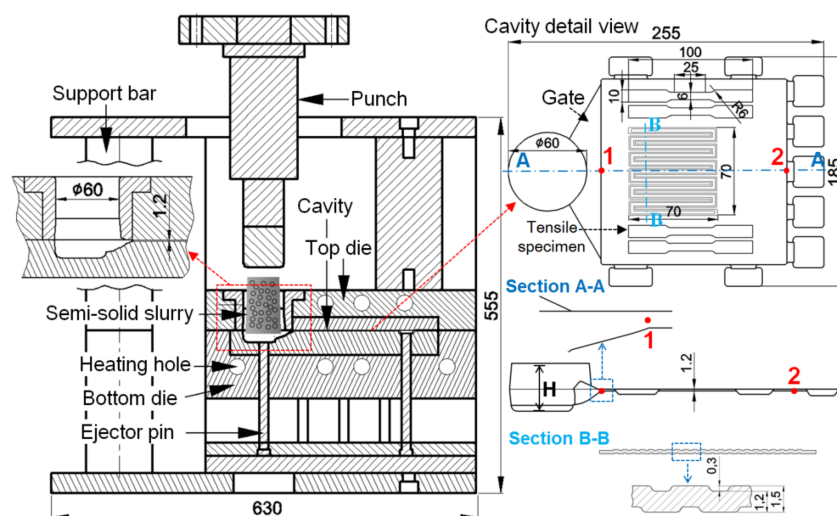


**Figure 2.** Schematic diagram of the compression die structure for forming thin plate and of the specimen position for investigating its microstructure and mechanical properties.

### 2.2.2. Parameters of the Forming Process

As regards the fabrication sequence of the thin plate using compression, firstly, the fabricated semi-solid billet was moved into the die. The semi-solid billet was then immediately compressed by dropping the punch. Next, the formed thin plate was removed from the die, and immediately cooled in water. The experiment conditions for thin plate fabrication through semi-solid billet compression with the punch are shown in Table 3. The compression experiment variables are classified into four categories: solid fraction of the semi-solid billet, cavity lubrication state, punch velocity, and punch pressure. A total of six experiments were configured. Conditions 1–3 involved different solid fractions of semi-solid billets. Graphite lubricant on the die cavity was used, with 300 mm/s of punch velocity and 200 MPa of punch pressure. For conditions 4–6, the parameters of condition 2 were used with the exception of one parameter. Specifically, the punch pressure was 100 MPa for condition 4, the punch velocity was 30 mm/s for condition 5, and, for condition 6, the graphite lubricant was not applied to the die cavity.

The friction factors ( $m$ ) with and without the graphite lubricant were obtained through a ring compression test. A ring shape with external diameter of 16 mm, internal diameter of 8 mm, and thickness of 5.33 mm was used. The ring specimen was preheated to 590 °C, and compression was then performed. Through the ring compression test, it was found that the friction factor for the graphite lubricant was 0.4, whereas a factor of 0.9 was measured when the graphite lubricant was omitted.

**Table 3.** Compression conditions in indirect forming of thin plates.

No.	Temperature (°C)/Solid Fraction (%) of Billets	Velocity, $V_p$ (mm/s)	Pressure, $P_p$ (MPa)	Friction Factor ( $m$ )
1	600/35	300	200	0.4
2 (standard)	590/45	300	200	0.4
3	578/55	300	200	0.4
4	590/45	300	100	0.4
5	590/45	30	200	0.4
6	590/45	300	200	0.9

### 2.3. Analysis of Microstructure and Mechanical Properties

#### 2.3.1. Microstructure

Since the semi-solid billet had a cylindrical shape of 55 mm in diameter and 90 mm in height, cooling occurred later at the center than at the edge when the billet was cooled in water. The billet microstructure was measured at a position close to the sample edge. The center of the semi-solid billet sample was cut in the horizontal direction, and a microstructure specimen was obtained from the cut billet, 2 mm from the edge.

To observe the microstructure of the thin plate, the gate of the thin plate was cut in the direction of section A-A, and the microstructure of the cut section (position 1) was measured (see Figure 2). To observe the behavior of the primary  $\alpha$ -Al particles, which were compressed and caused to flow into the cavity, the microstructure was measured at position 2. Along with the microstructure measurement, the equivalent diameter  $D$  and roundness  $R$  of the primary  $\alpha$ -Al particles were measured. The  $D$  value of a primary  $\alpha$ -Al particle is defined in Equation (1), while  $R$ , which indicates how close the primary  $\alpha$ -Al particle is to a circle, is defined in Equation (2). For a completely circular particle,  $R$  is 1, and this value increases with increased particle shape's irregularity,

$$D = \sqrt{\frac{4A}{\pi}} \quad (1)$$

$$R = \frac{p^2}{4\pi A} \quad (2)$$

where  $A$  is the area of a particle, and  $p$  is the perimeter of a particle.

### 2.3.2. Mechanical Properties

To analyze the formability of the thin plate in response to specific compression conditions, the height reduction ratio  $R_H$  was calculated using Equation (3). Note that a larger  $R_H$  indicates greater compression and shows that the formability is good.

$$R_H = \frac{H_0 - H}{H_0} \times 100 \quad (3)$$

In this formula,  $H_0$  is the height of the semi-solid billet sample, and  $H$  is the height of the compressed thin plate, as shown in section B-B of Figure 2.

As can be seen in the cavity detail view of Figure 2, a tensile test was conducted by fabricating a tensile test specimen at the side of the fabricated thin plate. Vickers hardness was measured for the tip of the tensile test specimen. This specimen was fabricated according to the ASTM E 8M, subsize standard, with a gage length of 25 mm and width of 6 mm. The specimen thickness was the thickness of the fabricated thin plate. The tensile test was conducted on the formed state, without any additional treatment, such as surface and thermal treatments. For the tensile test, 25 ton Material Testing System (MTS) equipment was used, and the strain rate was set to 1 mm/min. For accurate elongation measurements, the elongation was measured using an extensometer. For the Vickers hardness test, the load was set to 200 g. The measurements in the tensile test and Vickers hardness test were taken five times for each specimen.

## 3. Results

### 3.1. Microstructures of the Semi-Solid Billet

The temperature curve of the A356 alloy as a function of solidification time is shown in Figure 3. It can be seen that the time required for solidification at 578 °C (solid fraction of 55%) from the liquid state at 620 °C decreased as the stirring current increased. The solidification rate increases because the stirring velocity increases when the stirring current is raised. Without electromagnetic stirring, the time required for the sample to solidify at 578 °C was 247 s, while for 30, 60, and 90 A stirrings, 238, 227, and 191 s were required, respectively. In the 60 A case, the time necessary for solidification at 600 °C was 106 s, and the required time to decrease the temperature from 600 to 590 °C was 58 s.

Note that, when a molten metal is solidified through electromagnetic stirring, the stirring is stopped during solidification. The stirring is not conducted until the target temperature value is reached because the solidification progresses more quickly at the top surface and at the edge. When a stirring current of 60 A was applied, stirring was performed until a temperature of 611 °C was reached (for 36 s). From 611 to 578 °C, stirring was not performed. For the 30 and 90 A, stirring was performed until reaching 617 °C (for 29 s) and 611 °C (for 41 s), respectively. In other words, for higher stirring currents, the stirring is performed for a longer period of time until a lower temperature is reached. For the 60 and 90 A cases, the stirring was stopped when a solid fraction of approximately 20% was obtained, whereas, for the 30 A case, the stirring was stopped at 617 °C at a liquid state. This is because of the weak stirring force and temperature difference between the positions due to heat transfer during stirring. The billet temperature was measured at the center of the container when the semi-solid billet was fabricated, and a temperature difference of approximately 2.5 °C was obtained between the center and the edges of the billet. The stirring was stopped because the edge was at approximately 615 °C (12% solid fraction). Note that the stirring process was stopped as solidification progressed more quickly at the edge, but vibration persisted because of the continued effect of the electromagnetic field.

The microstructure of the stirred billets (60 A) and unstirred billets are shown in Figure 4. The stirred and unstirred samples exhibited significant differences, which were particularly noticeable between the various solid fractions. For the unstirred semi-solid billet, a dendrite structure was

dominant, while a fine globular structure was dominant for the stirred semi-solid billet. As the solid fraction increased, the primary  $\alpha$ -Al particles became coarser and more irregularly shaped.

The unstirred samples are shown in the left-hand side of Figure 4. For the billet with 35% solid fraction, it can be seen that the irregularly shaped primary  $\alpha$ -Al particles were arranged in a dendrite-type structure. In particular, it must be noted that the primary  $\alpha$ -Al particles were not attached to each other. In the billet with 45% solid fraction, coarse particles formed by the bonding of primary  $\alpha$ -Al particles could be seen, and the corners or tips of the irregular primary  $\alpha$ -Al particles were connected with each other. Newly created small, spherical primary  $\alpha$ -Al particles could also be seen. The billet with 55% solid fraction exhibited a coarse dendrite structure, in which irregular primary  $\alpha$ -Al particles were completely bonded, and the irregularly shaped primary  $\alpha$ -Al particles were arranged in a dendrite structure. As regards the microstructures of the unstirred billets, it could be seen that a dendrite structure was formed, as the irregularly shaped primary  $\alpha$ -Al particles arranged in a dendrite-type structure became bonded with each other.

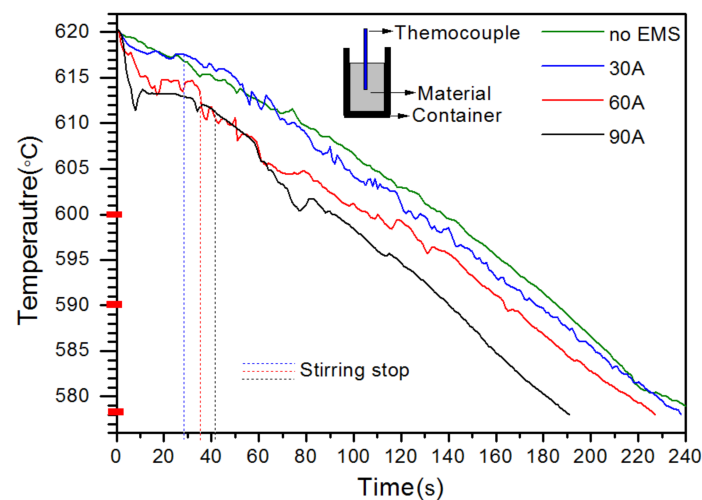


**Figure 3.** Solidification temperature according to the solidification time at different stirring currents.

The stirred samples are shown in the right-hand side of Figure 4. Only the small, spherical particles were distributed in the 35%-solid-fraction billet. The primary  $\alpha$ -Al particles in the billet with 45% solid fraction were coarse and irregularly shaped compared with those in the former case because of the bonding between the primary  $\alpha$ -Al particles and the particle growth. Further, the primary  $\alpha$ -Al particle shapes were coarser and more irregular in the billet with 55% solid fraction than in the 45%-solid-fraction billet. Globular particles could be observed in the billet with 55% solid fraction. The majority of the particles were rosettes, and some exhibited dendrite shapes formed by the bonding of the rosette particles.

Thus, the unstirred and stirred billets had dendrite and globular structures, respectively. This was due to the bonding of primary  $\alpha$ -Al particles in the unstirred case, and to the primary  $\alpha$ -Al particle motion by the liquid fluid flow in the stirred case. It has been observed that, when the solidification begins below the liquidus temperature, nuclei are generated with a dendrite structure arrangement and are separated by certain gaps without being bonded with each other. Nuclei are also generated without dendrite arrangement [13].

When solidified without stirring, starting above the liquidus temperature, the particles, that are initially organized in a dendrite structure arrangement, irregularly grow as the solidification proceeds and form a dendrite structure, as they bond with each other through diffusion. In the dendrite structure arrangement, because the angle grain boundary between the primary  $\alpha$ -Al particles is small, bonding between particles occurs more easily.

When solidified by stirring starting above the liquidus temperature, the primary  $\alpha$ -Al particles are moved by the liquid fluid flow, and the dendrite structure arrangement is broken. The primary  $\alpha$ -Al particles are deformed to spheroids by the liquid fluid and by wearing due to collisions between the particles. The electromagnetic field which continues to be applied even after stirring is stopped, generates vibration, and causes the primary  $\alpha$ -Al particles to move. Because of this vibration, primary  $\alpha$ -Al particle growth into irregular shapes is hindered [14].

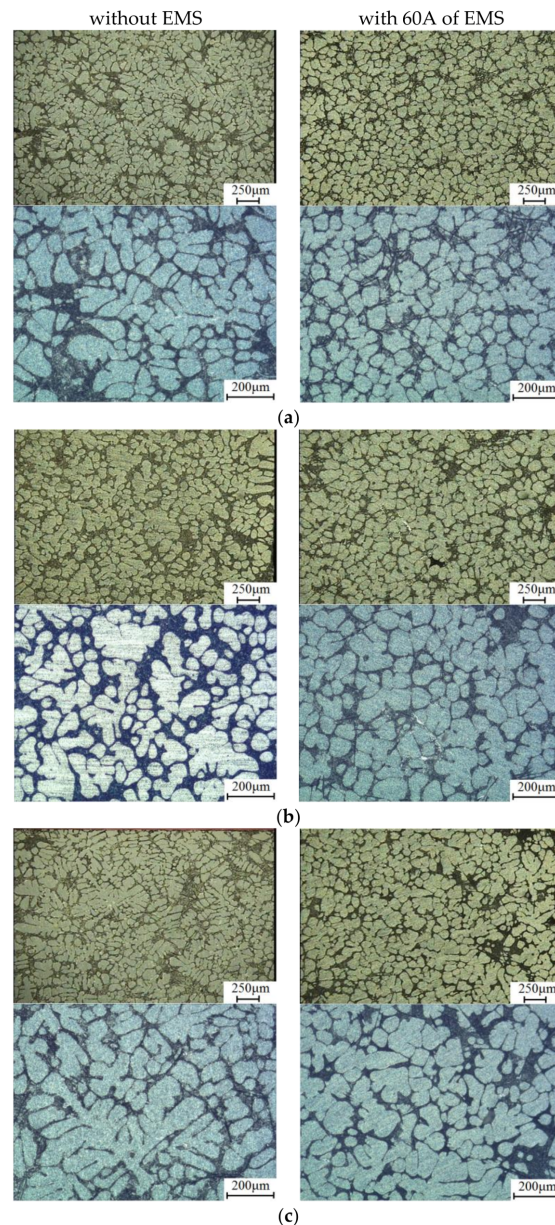


**Figure 4.** Microstructure of semi-solid billets with and without stirring: (a) 35% solid fraction; (b) 45% solid fraction; (c) 55% solid fraction.

The microstructures of the 45%-solid-fraction billets fabricated by stirring with 30 and 90 A, respectively, are shown in Figure 5. It can be seen that the primary  $\alpha$ -Al particles in the billet fabricated using 30 A were coarser than those in the billet fabricated with 60 A. The majority of the primary  $\alpha$ -Al particles were spheroids, but some dendrite shapes were present, in which rosette and irregularly shaped particles were bonded. From the microstructures presented in Figure 5b, it can be seen that the primary  $\alpha$ -Al particles were smaller and more globular in the billet fabricated with 90 A than

in that fabricated with 30 and 60 A (see Figure 4b). Rosette and dendrite-shaped particles were not present in the 90 A billet case. It can be seen that the particles with relatively irregular shapes were bonded with other particles at the corners. Because the stirring force and stirring velocity (shear strain rate) increased as the stirring current increased, the deformation of the primary  $\alpha$ -Al particles and the number of collisions between the particles increase and, thus, the primary  $\alpha$ -Al particles were deformed to become more globular. On the other hand, it can be seen that the bonding between the particles increased as a result of more frequent collisions between the particles.

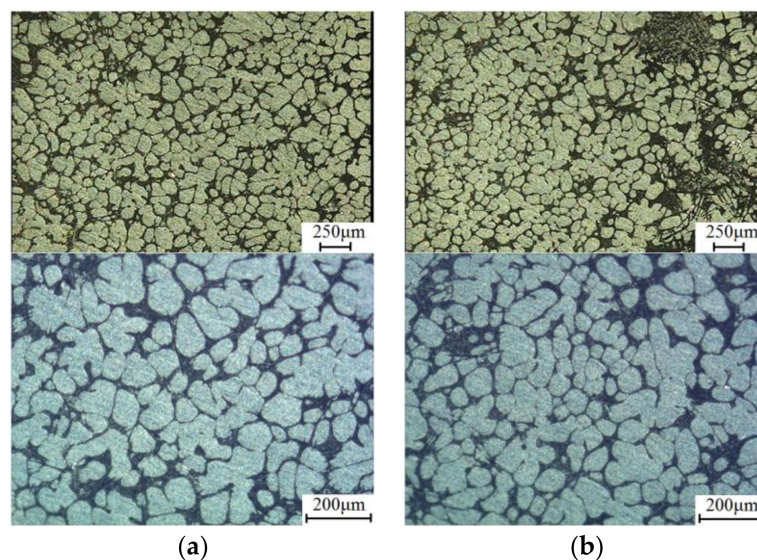


**Figure 5.** Microstructure of semi-solid billets with 45% solid fraction fabricated by different stirring currents: (a) 30 A of EMS; (b) 90 A of EMS. For 60 A of EMS A, see Figure 4b.

The  $D$  and  $R$  values of the primary  $\alpha$ -Al particles in the billets are shown in Figure 6. The  $D$  and  $R$  of the primary  $\alpha$ -Al particles were significantly smaller in the stirred billets than in the unstirred billets. As the solid fraction decreased and the stirring current increased, the  $D$  and  $R$  values of the primary  $\alpha$ -Al particles decreased.

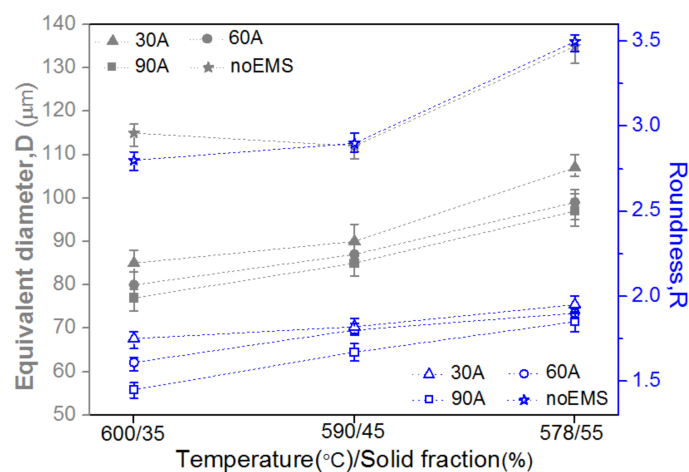


**Figure 6.** Equivalent diameter and roundness of primary  $\alpha$ -Al particles in semi-solid billets.

### 3.2. Microstructure of the Thin Plates

The microstructure of the thin plates fabricated by insertion of 60 A stirred billets into the die with graphite lubricant, compressing them with 200 MPa pressure at 300 mm/s velocity (conditions 1–3 of Table 3) is shown in Figure 7. The primary  $\alpha$ -Al particles were significantly smaller with much rounder shapes in all three thin plates, compared to the billets before compression (Figure 4). This is because a considerably large shear strain rate was applied by the punch compression, which caused the particles irregularly bonded with each other in the billet to become detached. The bonded particles, detached particles, single particles, and the residual liquid phase began to move because of the turbulent flow that occurred when they passed through the gate. At this point, the cross section was narrow, and the flow velocity increased significantly. Wearing of the particles occurred because of the collisions between them and as a result of the friction generated by the motion. Because of a large shear strain rate, bonding by collisions between particles did not occur. Similar to the observed billet microstructure (Figure 4), the microstructure of the thin plate fabricated with the 35%-solid-fraction billet had smaller and rounder particles than in the two other conditions. Considering the microstructure of the thin plate compressed with the 55%-solid-fraction billet shown in Figure 7c, a trace of rapidly expelled liquid phase could be confirmed at the bottom part of the gate (position 1). This phenomenon was due to the large bonding force between the particles and the low fluidity of the coarse particles. In the 55%-solid-fraction billet, because a large number of bonds existed between the particles, which were coarse, detachment and movement of the bonded particles were difficult even during compression. The same amount of liquid phase and solid phase could not move through the gate to the exterior simultaneously and, instead, a large amount of relatively good fluidity liquid phase exited the gate rapidly.

For all three conditions, the primary  $\alpha$ -Al particles were rounder and smaller at position 2 than at position 1. The number of primary  $\alpha$ -Al particles was small, and a large amount of eutectic structure could be confirmed, in which the liquid phase was filled. Because the distance over which the motion occurred was a little longer for the primary  $\alpha$ -Al particles at position 2 than for those at position 1, a larger amount of wear due to friction and collisions between the particles occurred. Because small and round particles have superior fluidity than coarse particles [15,16], the round and small particles exhibited greater motion than the coarse particles at position 2. Hence, the primary  $\alpha$ -Al particles of position 2 were smaller and rounder. The fluidity of the primary  $\alpha$ -Al particles was decreased because of the friction occurring during the movement and was further obstructed in the concavo-convex space. Therefore, the liquid phase, which had relatively excellent fluidity, moved faster than the primary  $\alpha$ -Al particles, and the eutectic structure occupied more space at position 2.

For the effect of the punch pressure, the microstructure of thin plates fabricated by insertion of 60 A stirred 45%-solid-fraction billets into the die with graphite lubricant, compressing them with 100 MPa pressure at 300 mm/s velocity (condition 4 of Table 3), is shown in Figure 8. The number of primary  $\alpha$ -Al particles was small at both positions 1 and 2, compared to the thin plate fabricated with 200 MPa shown in Figure 7b. Porosities were apparent at position 2. It could be determined that it was difficult for many of the primary  $\alpha$ -Al particles to move if a low punch pressure was applied during the compression of the semi-solid billet. The pressure compressing the semi-solid billet results in kinetic energy at the gate. The applied pressure of 100 MPa primarily caused the detachment of the bonded primary  $\alpha$ -Al particles in the semi-solid billet, while the force required to initiate the primary  $\alpha$ -Al particles motion became small. Therefore, many primary  $\alpha$ -Al particles could not pass the gate, and more liquid phase was moved, which filled the cavity.

For the effect of the punch velocity, the microstructure of thin plates fabricated by insertion of 60 A stirred 45%-solid-fraction billets into the die with graphite lubricant, compressing them with 200 MPa pressure at 30 mm/s velocity (condition 5 of Table 3), is shown in Figure 9. Compared to the thin plate fabricated at 300 mm/s velocity shown in Figure 7b, the sizes of the primary  $\alpha$ -Al particles were larger at both positions 1 and 2. At the position 1, primary  $\alpha$ -Al particles arranged in a dendrite shape could be seen. When the compression velocity applied to the semi-solid billet was low, the deformation was reduced, and the kinetic energy at the gate was reduced. The coarse and irregularly shaped primary

$\alpha$ -Al particles were almost unable to exit the gate at the narrow cross section. Relatively smaller primary  $\alpha$ -Al particles moved. For the moving primary  $\alpha$ -Al particles, round deformation occurred as a result of wearing due to friction during motion and collisions between the particles.

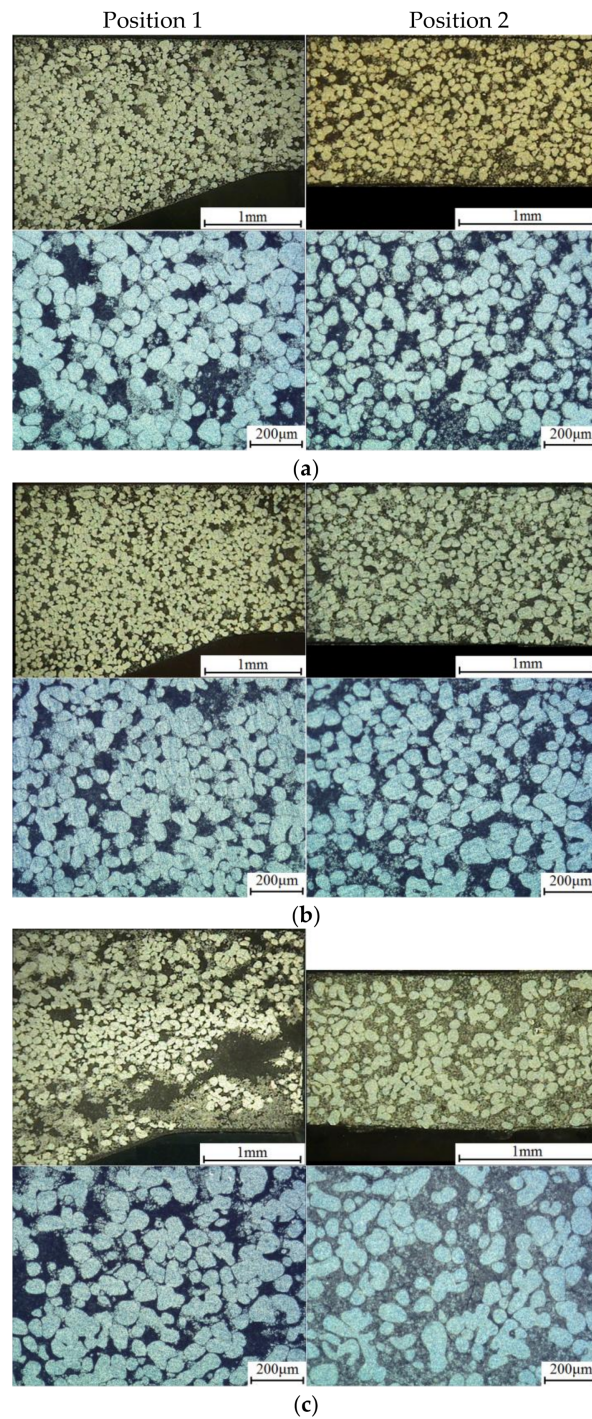


**Figure 7.** Microstructure of thin plates fabricated using 60 A stirred billets (graphite lubricant, 200 MPa of pressure and 300 mm/s of velocity): (a) Using a billet with 35% solid fraction; (b) Using a billet with 45% solid fraction; (c) Using a billet with 55% solid fraction.

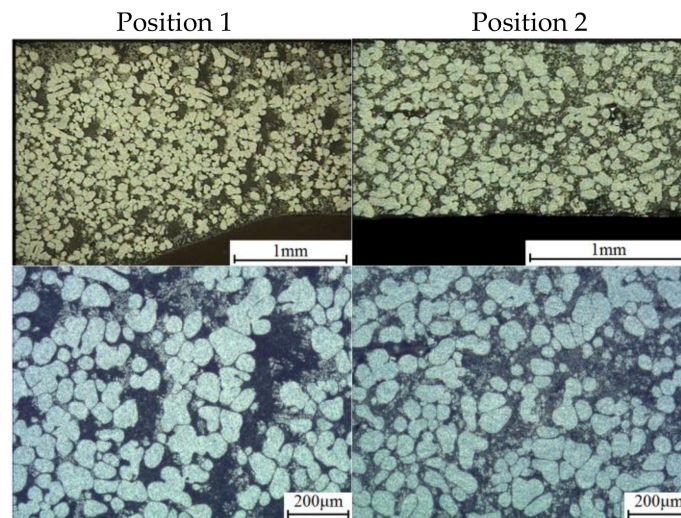


**Figure 8.** Microstructure of a thin plate fabricated using 60 A stirred 45%-solid-fraction billet, graphite lubricant, 100 MPa of pressure, and 300 mm/s velocity.

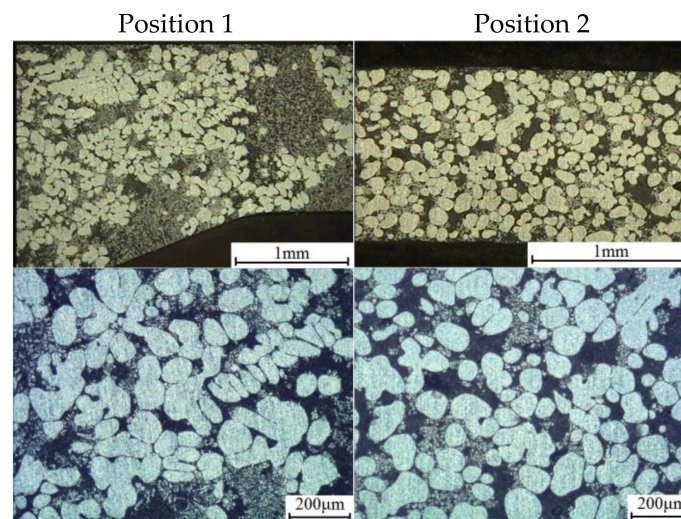


**Figure 9.** Microstructure of a thin plate fabricated using 60 A stirred 45%-solid-fraction billet, graphite lubricant, 200 MPa of pressure, and 30 mm/s velocity.

For the effect of the die friction, the microstructure of thin plates fabricated by insertion of 60 A stirred 45%-solid-fraction billets into the die, compressing them with 200 MPa pressure at 300 mm/s velocity (condition 6 of Table 3), is shown in Figure 10. At position 1, irregularly shaped primary  $\alpha$ -Al particles were condensed, and approximately half the substance was a eutectic structure of liquid phase. The microstructure at position 2 exhibited a primarily eutectic structure, and only several primary  $\alpha$ -Al particles were condensed. The friction factor of no graphite lubricant was 0.9, which was over two times greater than that of the graphite lubricant ( $m = 0.4$ ). If the friction of the die is large, almost no primary  $\alpha$ -Al particle can move, and only the liquid phase, which has relatively good fluidity, exits the gate. It must be noted that, because the primary  $\alpha$ -Al particles had an inter-particle bonding force, they were condensed in a lump shape in one position, despite the high flow velocity.

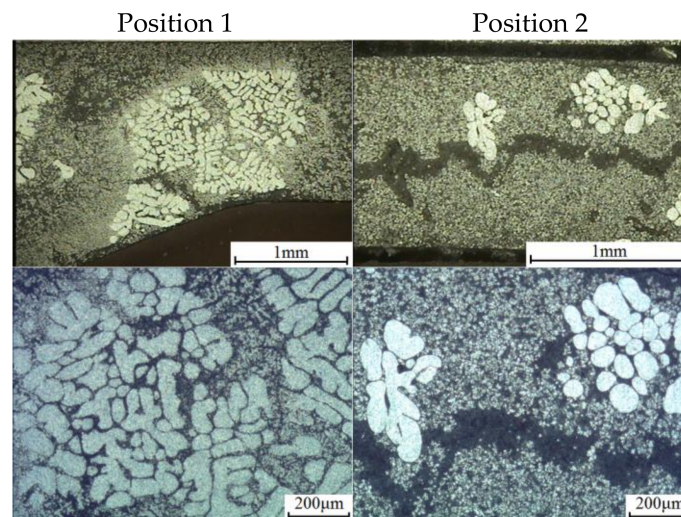


**Figure 10.** Microstructure of a thin plate fabricated using 60 A stirred 45%-solid-fraction billet, no graphite lubricant, 200 MPa of pressure, and 300 mm/s of velocity.

### 3.3. Formability and Mechanical Properties of the Thin Plates

The fabricated thin plate samples are shown in Figure 11. In the cases of conditions 1–3, where only the solid fractions of the billet were varied and the remaining compression conditions were identical, the  $H$  values were 17, 21, and 24 mm for condition 1 (35% solid fraction), condition 2 (45% solid fraction), and condition 3 (55% solid fraction) billets, respectively, while the height reduction ratio  $R_H$  was 81.1%, 76.6%, and 73.3%, respectively. In the sample fabricated under condition 3, an unformed part existed, and a flash phenomenon occurred at the compressed part. It is apparent that the compression was not well-performed, as the solid fraction of the billet increased, and a large number of solid particles were evident. Hence, the formability was degraded. The  $H$  and  $R_H$  of the sample fabricated under condition 4 were 27 mm and 70%, respectively. The  $H$  and  $R_H$  of the sample fabricated under condition 5 were 30 mm and 66.6%, respectively. Nonforming occurred in this sample. In the samples fabricated under conditions 4 and 5, the  $H$  was the highest obtained value for all conditions. It can be seen that velocity and pressure were the factors with the greatest effect on compressibility (formability). As regards compression condition 6, the  $H$  and  $R_H$  of the compressed part were 23 mm and 74.4%, respectively. Although a large amount of material was compressed in this case compared to the other conditions (as shown in Figure 10), this was filled with the liquid phase that flowed out from the billet only. Also, it was confirmed that a flash phenomenon occurred in the compressed part in this case, because of the rapid discharge of the liquid phase.

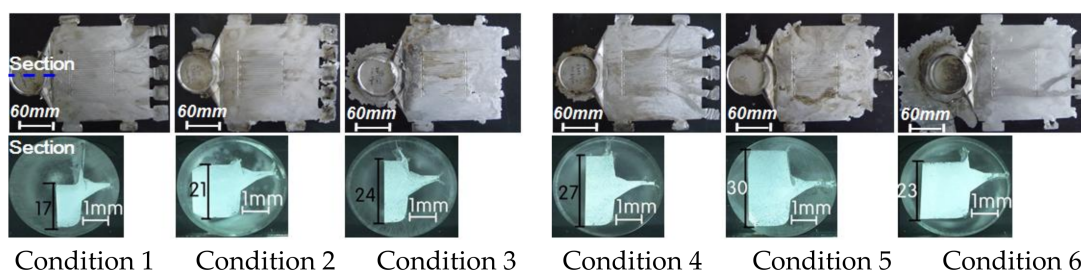


**Figure 11.** Thin plate samples fabricated in different compression conditions.

The mechanical properties of the thin plates fabricated under the six compression conditions are shown in Table 4. The tensile strength and elongation of conditions 1 and 2 were higher than those

of the other conditions. The tensile strength of condition 2 was 205 MPa and the elongation was 8%, which was the highest obtained value. For condition 6, tensile strength and elongation were the lowest, and Vickers hardness was the highest because there were almost no primary  $\alpha$ -Al particles, as shown in Figure 10, and there was only a eutectic structure filled with a liquid phase; thus, high brittleness was exhibited.

**Table 4.** Mechanical properties of thin plates fabricated in different compression conditions.

No.	Ultimate Tensile Strength (MPa)			Elongation (%)			Vickers Hardness (HV)		
	Mean	Max.	Min.	Mean	Max.	Min.	Mean	Max.	Min.
1	190	202	186	7	9	6	64	66	63
2	205	210	198	8	10	7	65	66	64
3	188	192	185	5	6	4	66	68	65
4	175	181	170	6	7	5	67	69	65
5	160	165	154	6	7	6	62	65	61
6	125	130	122	3	3	2	89	90	87

#### 4. Conclusions

Semi-solid billets were fabricated by electromagnetic stirring, and experiments were conducted involving the fabrication of thin plates through compression of the billets. From these experiments, the effect of stirring on particle growth and the behavior of the particles by the compression were examined.

- (1) For unstirred semi-solid billets, a dendrite structure was dominant, while a fine globular structure was dominant for the stirred semi-solid billets. As the solid fraction increased, the primary  $\alpha$ -Al particles became coarser and more irregularly shaped.
- (2) The equivalent diameter and roundness of the primary  $\alpha$ -Al particles were significantly smaller in the stirred billets than in the unstirred billets. As the solid fraction decreased, and the stirring current increased, the equivalent diameter and roundness of the primary  $\alpha$ -Al particles decreased.
- (3) The primary  $\alpha$ -Al particle sizes were reduced as the compressing velocity was increased, while a greater number of particles could be moved if the compressing pressure was increased. As the path over which the motion occurred became smoother, the fluidity of the particles improved.
- (4) As a group of primary bonded  $\alpha$ -Al particles was compressed under a large strain rate, the bonds were broken, and the group separated into individual particles. When the primary  $\alpha$ -Al particles and residual liquid phase passed through a gate, at which the cross section was narrow, the flow velocity increased significantly, and the particles experienced turbulent flow. As wearing caused by friction and inter-particle collisions during this motion occurred, the particle shapes became increasingly spherical, because the particle sizes decreased, and the corner curvatures were increased. As the distance over which the particles moved increased, the particles were reduced in size and became more spherical.

**Acknowledgments:** This work was supported by Kyungnam University Foundation Grant, 2017.

**Author Contributions:** Chul Kyu Jin designed the experiment tools, performed the experiment, analysed the experimental results, and has contributed to the discussions as well as revisions.

**Conflicts of Interest:** The author declares no conflict of interest.

#### References

1. Metz, S.A.; Flemings, M.C. *Fundamental Study of Hot Tearing*; American Foundrymen's Society: Schaumburg, IL, USA, 1970; Volume 78, pp. 453–460.
2. Spencer, D.B.; Mehrabian, R.; Flemings, M.C. Rheological Behavior of Sn-15 Pct Pb in the Crystallization Range. *Metall. Mater. Trans. A* **1972**, *3*, 1925–1932. [[CrossRef](#)]

3. Fan, Z.; Fang, X.; Ji, S. Microstructure and mechanical properties of rheo-diecast (RDC) aluminium alloys. *Mater. Sci. Eng. A* **2005**, *412*, 298–306. [[CrossRef](#)]
4. Biswas, B.; Hermann, R.; Das, J.; Priede, J.; Gerbeth, G.; Acker, J. Tailoring the microstructure and mechanical properties of Ti–Al alloy using a novel electromagnetic stirring method. *Scr. Mater.* **2006**, *55*, 1143–1146. [[CrossRef](#)]
5. Nafisi, S.; Emadi, D.; Shehata, M.T.; Ghomashchi, R. Effects of electromagnetic stirring and superheat on the microstructural characteristics of Al–Si–Fe alloy. *Mater. Sci. Eng. A* **2006**, *432*, 71–83. [[CrossRef](#)]
6. Bae, J.B.; Kim, T.W.; Kang, C.G. Experimental investigation for rheology forming process of Al–7% Si aluminum alloy with electromagnetic system. *J. Mater. Process. Technol.* **2007**, *191*, 165–169. [[CrossRef](#)]
7. Tzimas, E.; Zavaliangos, A. A comparative characterization of near-equiaxed microstructures as produced by spray casting, magnetohydrodynamic casting and the stress induced, melt activated process. *Mater. Sci. Eng. A* **2000**, *289*, 217–227. [[CrossRef](#)]
8. Haga, T.; Suzuki, S. Casting of aluminum alloy ingot for thixoforming using a cooling slope. *J. Mater. Process. Technol.* **2001**, *118*, 161–172. [[CrossRef](#)]
9. Zhang, Z.; Li, J.; Yue, H.; Zhang, J.; Li, T. Microstructure evolution of A356 alloy under compound field. *J. Alloy. Compd.* **2009**, *484*, 458–462. [[CrossRef](#)]
10. Canyook, R.; Wannasin, J.; Wisuthmethangkul, S.; Flemings, M.C. Characterization of flow behavior of semi-solid slurries containing low solid fractions in high-pressure die casting. *Acta Mater.* **2012**, *60*, 3501–3510. [[CrossRef](#)]
11. Nafisi, S.; Lashkari, O.; Ghomashchi, R.; Ajersch, F.; Charette, A. Microstructure and rheological behavior of grain refined and modified semi-solid A356 Al–Si slurries. *Acta Mater.* **2006**, *54*, 3503–3511.
12. Oh, S.W.; Bae, J.B.; Kang, C.G. Effect of Electromagnetic Stirring Conditions on Grain Size Characteristic of Wrought Aluminum for Rheo-forging. *J. Mater. Eng. Perform.* **2008**, *17*, 57–63. [[CrossRef](#)]
13. Flemings, M.C. Solidification processing. *Metall. Trans.* **1974**, *5*, 2121–2134. [[CrossRef](#)]
14. Hunt, J.D.; Jackson, K.A. Nucleation of solid in an undercooled liquid. *J. Appl. Phys.* **1966**, *37*, 254–257. [[CrossRef](#)]
15. Seo, P.K.; Kim, D.U.; Kang, C.G. The effect of the gate shape on the microstructural characteristic of the grain size of Al–Si alloy in the semi-solid die casting process. *Mater. Sci. Eng. A* **2007**, *445–446*, 20–30. [[CrossRef](#)]
16. Matsumiya, T.; Flemings, M.C. Modeling of Continuous Strip Production by Rheocasting. *Metall. Trans. B* **1981**, *12B*, 17–31. [[CrossRef](#)]



© 2018 by the author. Licensee MDPI, Basel, Switzerland. This article is an open access article distributed under the terms and conditions of the Creative Commons Attribution (CC BY) license (<http://creativecommons.org/licenses/by/4.0/>).